Research Article

Segregation of Cu-In-S Elements in the Spray-Pyrolysis-Deposited Layer of CIS Solar Cells

Seigo Ito and Toshihiro Ryo

Department of Electric Engineering and Computer Sciences and Department of Materials Science and Chemistry,
University of Hyogo, 2167 Shosha, Himeji, Hyogo 671-2280, Japan

Correspondence should be addressed to Seigo Ito, itou@eng.u-hyogo.ac.jp

We report the fabrication of superstrate-structured solar cells by the deposition of Cu-In-S (CIS) films on ⟨glass/FTO/TiO$_2$/In$_2$S$_3$⟩ under air by spray pyrolysis. The cells had an open-circuit voltage of 0.551 V, a photocurrent density of 9.5 mA/cm^2, a fill factor of 0.45, and a conversion efficiency of 2.14%. However, transmission electron microscopy/energy dispersive X-ray (TEM-EDX) analysis revealed significant differences between the atomic ratio of the setting material in the spray-deposition solution and the elements in the layer. Moreover, TEM-EDX measurements suggested strong segregation of the Cu-In-S elements in the spray-pyrolysis-deposited layer. The degree of segregation depended on the substrate (⟨glass⟩, ⟨glass/TiO$_2$⟩, or ⟨glass/TiO$_2$/In$_2$S$_3$⟩), although Cu$_3$In$_5$S$_9$ nanoparticles were segregated in the sulfur layer.

1. Introduction

Compound solar cells with high-conversion efficiencies (20.3%) have been fabricated by vacuum methods [1], which are slow and require costly equipment. Nonvacuum processes for solar cell materials, such as Cu(In$_{1-x}$Ga$_x$)Se$_2$, CuInSe$_2$, and CuInS$_2$ (CIS), have been investigated with the aim of developing fast and inexpensive fabrication methods. Printing [2, 3], spray-pyrolysis-deposition (SPD) [4, 5], selenization of printed metal oxides with H$_2$S or H$_2$Se [6], and electrochemical deposition [7, 8] have been explored as alternative methods. Less toxic materials are required because nonvacuum methods are carried out in air; therefore CuInS$_2$ absorber materials are more suitable than CuInSe$_2$ or Cu(In,Ga)Se$_2$. This is particularly important for SPD methods because aerosols are formed from the compounds. In this work, the structures of spray-pyrolysis-deposited Cu-In-S layers, which have 2.14% conversion efficiency in superstrate-structured solar cells, were studied by transmission electron microscopy-energy dispersive X-ray (TEM-EDX) analysis. It was confirmed that SPD formed a segregated structure in the Cu-In-S layers and the Cu-In-S structure differed between substrates.

2. Experimental

Cu-In-S films were deposited on substrates at 300°C in air, by SPD. The substrates were glass, ⟨glass/TiO$_2$⟩, and ⟨glass/TiO$_2$/In$_2$S$_3$⟩. Figure 1 shows the fabrication processes for the Cu-In-S layer and the resulting Cu-In-S structures. The glass substrates were coated with a TiO$_2$ layer (t = 100 nm) by SPD at 400°C. The solution used for depositing the TiO$_2$ compact layer was a mixture of titanium acetylacetonate (TAA) and ethanol (9 : 1 v/v). TAA was prepared by slowly injecting acetylacetone (99.5%, Kanto Chemical Co. Inc., Tokyo, Japan) into titanium tetraisopropoxide (97%, Kanto Chemical Co. Inc.) at a mole ratio of 2 : 1. The In$_2$S$_3$ layers (t = 100 nm) were used as the buffer layers and deposited using a precursor solution of InCl$_3$ (10 mM) and thiourea (20 mM) in water (10 mL) at 300°C. The Cu-In-S spray deposition was performed using an aqueous solution of CuCl$_2 \cdot$2H$_2$O (30 mM; 97.5%, Kanto Chemical Co.), InCl$_3$ (30 mM; 98%, Kishida Chemical Co., Ltd, Japan) and thiourea (150 mM; Tokyo Chemical Industry Co., Ltd, Tokyo, Japan) giving a Cu/In/S ratio of 1 : 1 : 5. The Cu-In-S absorber layer was deposited by spraying the Cu-In-S SPD solution (40 mL) on to each substrate at 300°C at a speed of 2 mL min^{-1}. The Cu-In-S layers were scratched
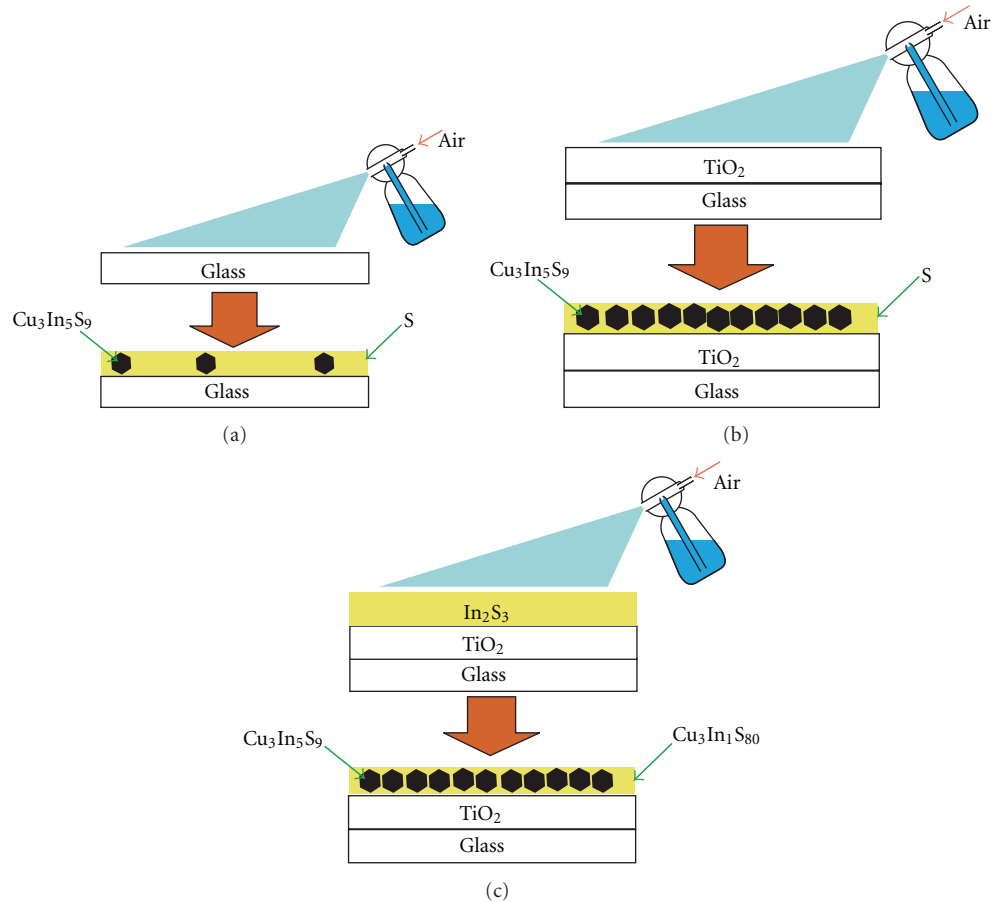
Figure 1: Relations between substrates, (a) glass, (b) glass/TiO_2, and (c) glass/TiO_2/In_2S_3, and the structures of spray-pyrolysis-deposited Cu-In-S.

from the substrates and powdered, dispersed in ethanol, and attached to Mo grids for TEM observation. A TEM-EDX system (JEOL JEM2100) was used to characterize the Cu-In-S materials. XPS analysis conducted previously showed an oxidation state just on the Cu-In-S surface [5]. Thus, the powdered Cu-In-S samples for TEM observation show the inside of the SPD layer.

SEM cross-section images showed that the surface is relatively flat [5] with a roughness factor of only 1. However, there were several pinholes due to dust and aggregates. Moreover, observation by atomic scale view indicated a very rough surface because it is not a single crystal layer, hence the superstrate-type structure of the solar cells has been fabricated.

The back contact electrode formed from an Au layer deposited by vacuum evaporation produced superstrate-structured solar cells ⟨glass/F-doped SnO$_2$ (FTO)/TiO$_2$/Cu-In-S/Au⟩. The samples used to obtain the photo I-V curve were 5 mm × 5 mm. The photovoltaic measurements employed an AM 1.5 solar simulator equipped with a xenon lamp (YSS-100A, Yamashita Denso, Japan). The power of the simulated light was calibrated to 100 mW cm^{-2} by using a reference Si photodiode (Bunkou Keiki, Japan). The I-V curves were obtained by applying an external bias to the cell

and measuring the generated photocurrent with a DC voltage current source (6240, ADCMT, Japan). It is very important to obtain information regarding the electrical properties of samples on various substrates for the preparation of Cu-In-S solar cells. However, since the resistance of the Cu-In-S layer was very high, the electrical resistance and the Hall effects could not be measured.

3. Results and Discussion

Figure 2 shows the photo and dark I-V curves for the superstrate-structured solar cell ⟨glass/FTO/TiO$_2$/In$_2$S$_3$/Cu-In-S/Au⟩ fabricated by SPD. The crossing of the curves suggests double-diode effects in the CIS solar cells. The open-circuit photovoltage, the short-circuit photocurrent density, the fill factor, and the conversion efficiency were 0.521 V, 9.68 mA cm^{-2}, 0.423, and 2.14%, respectively, and were improvements compared with our previous report [5], obtained by optimizing the SPD conditions. The conversion efficiency is far removed from the best Cu-based solar cells (20.1%) [1]; however, if the efficiency of SPD-processed solar cells can be enhanced by over 10% in the near future, this would be a very significant improvement due to the high-speed and nonvacuum processing methods used in
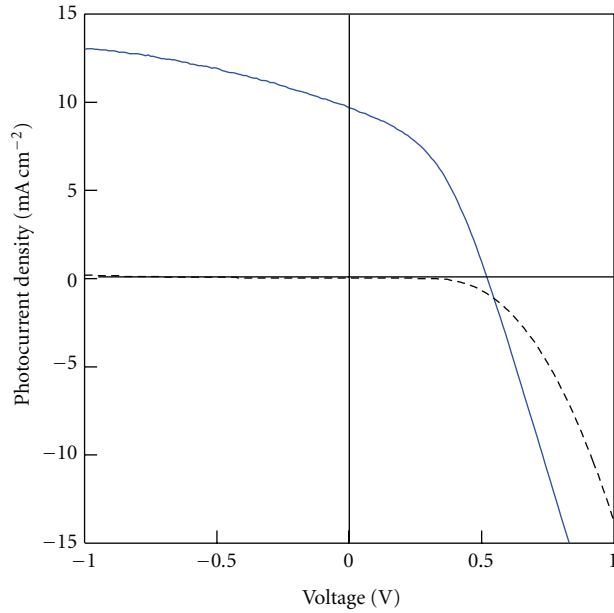
FIGURE 2: Photo (solid) and dark (dashed) I-V curves for the $\langle$glass/FTO/TiO$_2$/In$_2$S$_3$/Cu-In-S/Au$\rangle$ solar cell. The cell size was 5 mm $\times$ 5 mm, and the cell was irradiated with AM 1.5 (100 mW cm^{-2}) light.
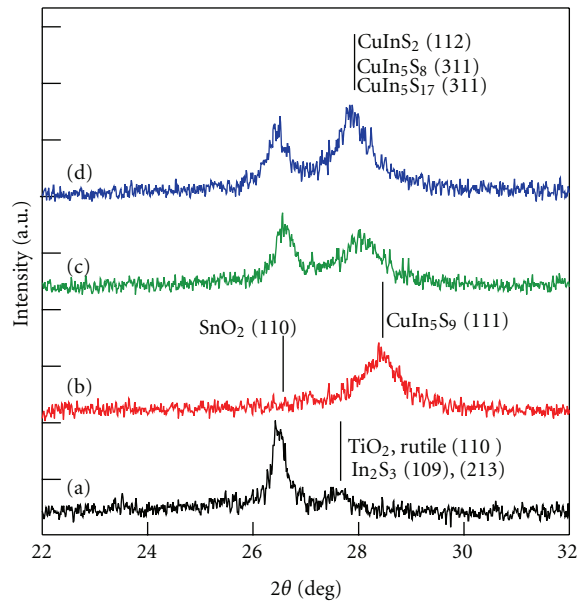
FIGURE 3: XRD patterns of $\langle$glass/FTO/TiO$_2$/In$_2$S$_3\rangle$ (a), $\langle$glass/Cu-In-S$\rangle$ (b), $\langle$glass/FTO/TiO$_2$/Cu-In-S$\rangle$ (c), and $\langle$glass/FTO/TiO$_2$/In$_2$S$_3$/Cu-In-S$\rangle$ (d). Numbers in round brackets show the crystal plane of materials in reference to JCPDS card data.

the fabrication of cost-effective solar cells. Thus, further investigation is required to improve the conversion efficiency. Here, we report changes in the CIS layer as observed by XRD and TEM-EDX.

Figure 3 shows the XRD patterns for the Cu-In-S layers on the different substrates that produced the $\langle$glass/Cu-In-S$\rangle$, $\langle$glass/FTO/TiO$_2$/Cu-In-S$\rangle$, and $\langle$glass/

FTO/TiO$_2$/In$_2$S$_3$/Cu-In-S$\rangle$ structures. The peak at 26.4° was attributed to SnO$_2$ (26.6° by JCPDS 88–0287) in FTO (Figure 3(a)); therefore, an SnO$_2$ peak was not observed in the XRD pattern of Cu-In-S on the glass substrate (Figure 3(b)). The peak at 27.6° in Figure 3(a) was assigned to In$_2$S$_3$ (27.4° by JCPDS 73–1366) and TiO$_2$ (27.7° by JCPDS 88–1173) and was not observed
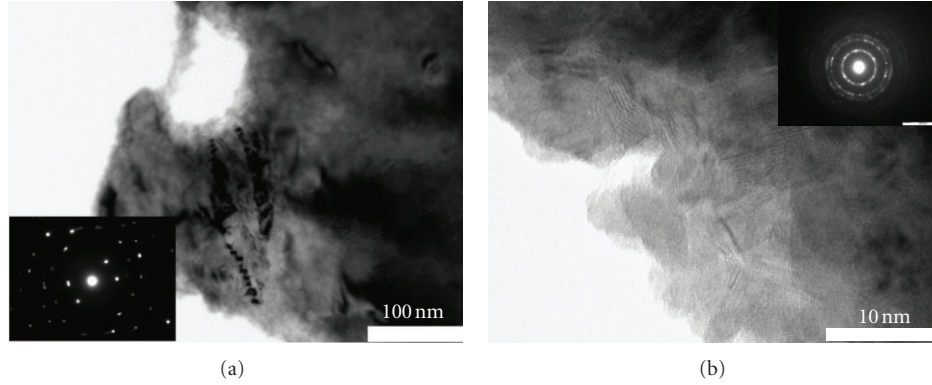
FIGURE 4: TEM image of spray-pyrolysis-deposited Cu-In-S with the electron diffusion patterns (inset) on a glass substrate: (a) the major part and (b) the minor part.
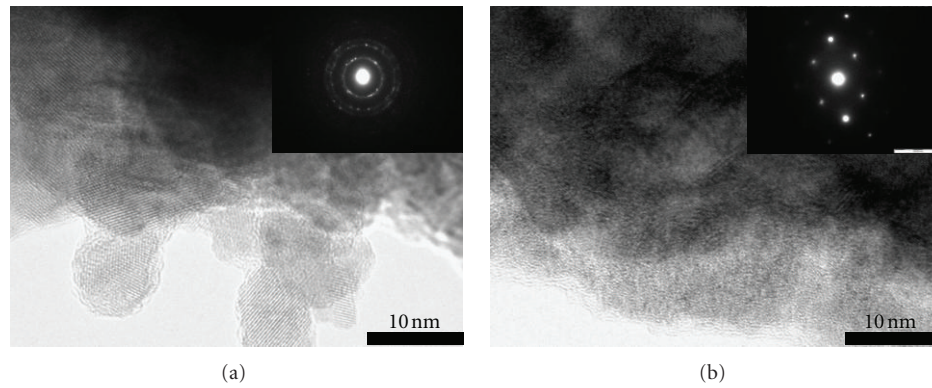

FIGURE 5: TEM image of spray-pyrolysis-deposited Cu-In-S with the electron diffusion patterns (inset) on a glass/TiO_2 substrate: (a) the major part and (b) the minor part.

TABLE 1: The atomic ratios of Cu-In-S analyzed by TEM-EDX. Each location is indicated by the relevant figure number.

Substrate	Major/Minor	Cu	In	S	Figures
⟨glass⟩	Major	0.06	0.00	99.94	Figure 4(a)
	Minor	16.00	28.41	55.58	Figure 4(b)
⟨glass/TiO_2⟩	Major	16.49	30.49	53.02	Figure 5(a)
	Minor	0.19	0.25	99.56	Figure 5(b)
⟨glass/TiO_2/In_2S_3⟩	Major	17.85	29.51	52.65	Figure 6(a)
	Minor	3.78	1.17	95.05	Figure 6(b)

in the ⟨glass/FTO/TiO_2/In_2S_3/Cu-In-S⟩ (Figure 3(c)) and ⟨glass/FTO/TiO_2/In_2S_3/Cu-In-S⟩ (Figure 3(d)) XRD patterns. Hence, the In_2S_3 layer had diffused into the Cu-In-S layer, confirmed by EPMA mapping analysis of the cross-sectional image [5]. The TiO_2 peak was buried below the Cu-In-S layer (Figure 3(c)) because of the very thin TiO_2 layer (t = 200 nm) and made evident by the small XRD signal.

Although the positions of the peaks were very close to the $CuInS_2$ peak (27.9° by JCPDS: 85–1575), the Cu-In-S XRD peaks (27.8–28.4°) varied significantly among substrates (Figures 3(b)–3(d)) and the peak shifts suggested variations in the types of Cu-In-S crystals. Due to the large

ratio of sulfur in the Cu-In-S layer (Cu-poor), which will be addressed in the TEM-EDX discussion to follow, assignment of the peaks from 27.8° to 28.4° in Figures 3(b)–3(d) would be $CuIn_{11}S_{17}$ (27.7° by JCPDS: 34–0797), $CuIn_5S_8$ (27.7° by JCPDS: 72–0956), and $CuIn_5S_9$ (28.4° by JCPDS: 49–1383). Therefore, it was thought that the peak shifts may be due to variations in the Cu-In-S crystals, which are projecting the compositions of the Cu-In-S.

The elemental analysis of Cu-In-S by TEM-EDX is shown in Table 1 and the locations analyzed are shown in Figures 4, 5, and 6. The Cu-In-S samples for TEM-EDX analysis were taken from the layers deposited on the different substrates: glass, glass/TiO_2, and glass/TiO_2/In_2S_3. It was confirmed that the Cu-In-S elements were segregated in the SPD layer. The components of the Cu-In-S materials were $CuInS_2$, $Cu_3In_5S_9$, $Cu_2In_4S_7$, $CuIn_3S_5$, and $CuIn_5S_8$ [9] with atomic ratios calculated as 25.00 : 25.00 : 50.00, 17.65 : 29.41 : 52.94, 15.38 : 30.77 : 53.85, 11.11 : 33.33 : 55.56, and 7.14 : 35.71 : 57.14, respectively. Therefore, the Cu-poor and In-rich portions of the segregated Cu-In-S layer were close to the composition ratio of $Cu_3In_5S_9$.

Figure 4 shows the TEM images of Cu-In-S deposited on a glass substrate. It was confirmed that, although the spray-pyrolysis solution for the Cu-In-S layer contained a
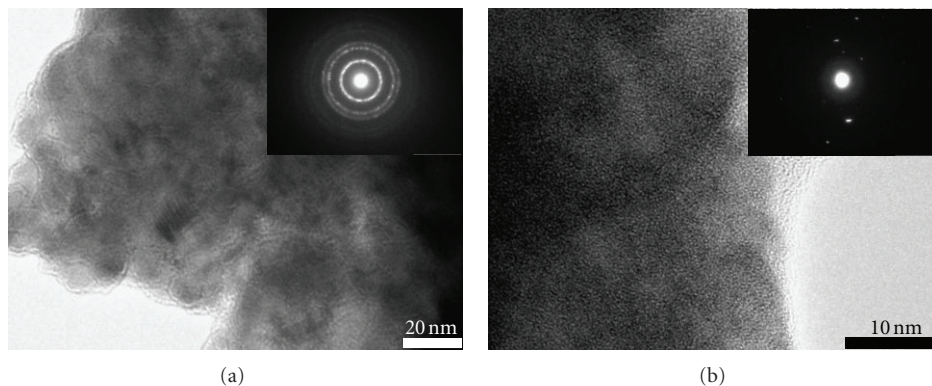
(a)   (b)

FIGURE 6: TEM image of spray-pyrolysis-deposited Cu-In-S with the electron diffusion patterns (inset) on a glass/TiO$_2$/In$_2$S$_3$ substrate: (a) the major part and (b) the minor part.

significant amount of copper and indium, the layer on the glass substrate was mainly pure sulfur (Figure 4(a), Table 1). The sulfur particles were several hundred nanometers in size. The atomic lattice was not visible in the TEM images because sulfur is much lighter than the heavy metal elements. However, the electron scattering patterns showed a single crystal (inset, Figure 4(a)). A small number of nanoparticles around 10 nm in diameter were observed (Figure 4(b)) and revealed the atomic lattice because they contained metallic elements. The electron sputtering pattern (inset, Figure 4(b)) suggested the existence of a polycrystalline structure. EDX analysis indicated that the Cu-In-S elemental ratio was close to Cu$_3$In$_5$S$_9$. Hence, a considerable amount of the copper metal source (CuCl$_2$) did not end up in the Cu-In-S layer and was dispersed somewhere else during SPD. The structure of the Cu-In-S layer (Figure 1(a)) shows the segregated Cu$_3$In$_5$S$_9$ particles in the sulfur layer.

Figure 5 shows the TEM images of Cu-In-S deposited on a glass/TiO$_2$ substrate. In contrast to the glass substrate (Figure 4), most of the Cu-In-S layer consisted of Cu$_3$In$_5$S$_9$ nanocrystals, 10 nm in diameter (Figure 5(a)). The electron diffraction pattern also suggested it had a nanocrystalline structure. Again the heavy metal elements meant that the nanocrystal atomic lattice could be observed. Although the nanocrystals contained copper, the Cu/In ratio was only 0.54 : 1, which was half that of the setting ratio (1 : 1) in the spray-deposition solution. The CuCl$_2$ in the Cu-In-S solution was again dispersed and not deposited in the Cu-In-S layer. In the minor part of Cu-In-S layer, a small amount of copper was observed (Figure 5(b)). However, when the substrate was changed from glass to glass/TiO$_2$, the amount of metal ([Cu + In]/[Cu + In + S]) in the sulfur rich part increased from 0.06% (Figure 4(a)) to 0.44% (Figure 5(b)). The electron scattering suggested a single crystal (inset, Figure 5(b)), although an atomic lattice was not observed, which may be because sulfur is a light element. Therefore, it was concluded that the substrate (⟨glass⟩ or ⟨glass/TiO$_2$⟩) significantly affected the composition and structure of the spray-pyrolysis-deposited CuInSe$_2$ layer. The structure of Cu-In-S layer deposited on the glass/TiO$_2$ substrate by spray pyrolysis is shown in Figure 1(b).

Figure 6 shows the TEM images of Cu-In-Se deposited on a glass/TiO$_2$/In$_2$S$_3$ substrate. The atomic ratio showed that, for Cu-In-Se, the layer mainly consisted of Cu$_3$In$_5$S$_9$ (Figure 6(a)), although a small amount of Cu$_3$In$_1$S$_{80}$ (Figure 6(b)) was present. Pure sulfur (Figures 4(a) and 5(b)) was not observed because of the In$_2$S$_3$ buffer layer and interdiffusion to the upper Cu-In-S layer. Cu$_3$In$_5$S$_9$ was present as nanocrystals, around 10 nm in diameter (Figure 6(a)), and the electron diffraction pattern suggested a polycrystalline structure (inset, Figure 6(a)). The Cu$_3$In$_1$S$_{80}$ particles were around several hundred nanometers in size (Figure 6(b)) and the atomic lattice was not visible because of the light sulfur atoms, although the electron diffraction pattern suggests a single-crystalline structure (inset, Figure 6(b)). Therefore, Cu-In-S was segregated as Cu$_3$In$_5$S$_9$ and Cu$_3$In$_1$S$_{80}$. The structure of the Cu-In-S layer deposited on the glass/TiO$_2$/In$_2$S$_3$ substrate by spray pyrolysis is shown in Figure 1(c).

The ratios of Cu-In-S, such as Cu$_3$In$_5$S$_9$ and Cu$_3$In$_1$S$_{80}$, simply show integral multiplication of the TEM-XRD results of Table 1. From a scientific point of view, the crystal structures should be revealed by XRD analysis. However, the results from normal XRD were obscure and GIXRD may be a more suitable method. Nevertheless, although GIXRD may have provided better results, the Cu-In-S was a mixture of small crystals and amorphous phases of different Cu-In-S compositions, making crystal identification in this work very complicated. It would be desirable to improve the analytical methods in the future.

4. Conclusions

Compound solar cells based on Cu-In-S (CIS) were prepared by SPD under air. Although the Cu-In-S layer had a segregated structure, the solar cells had a 9.68 mA cm^{-2} short-circuit photocurrent density and 2.14% conversion efficiency. The segregated structures differed among substrates. The resulting Cu-In-S layers were copper poor due to the loss of CuCl$_2$ during SPD. Therefore, the next step in improving the conversion efficiency is to control the amount of copper in the Cu-In-S layer. Since the significance of the

contribution of a Cu-poor $CuInS_2$ and $CuInSe_2$ solar cells has been discussed in the publications [10, 11], we believe that a Cu-poor $CuInS_2$ layer, and hence the presence of $Cu_3In_5S_9$, may contribute to the photovoltaic effects.

Samples prepared for this kind of work may be solid mixtures of $CuInS_2$, $CuIn_3S_5$, and so on and should be clearly identified. Each major part of the sample was expressed in the TEM figures in this paper. It is very difficult to obtain the exact components of such segregated materials by other methods, such as XPS, Auger, SIMS, Raman, XRD, and EPMA, because the resolutions in these methods reach the submicron range and give mixed information about major and minor parts of the materials. Advancements in the analytical tools may reveal further details in the future.

Acknowledgment

References

[1] P. Jackson, D. Hariskos, E. Lotter et al., "New world record efficiency for Cu(In, Ga)Se$_2$ thin-film solar cells beyond 20%," *Progress in Photovoltaics: Research and Applications*, vol. 19, no. 7, pp. 894–897, 2011.

[2] B. M. Sager, D. Yu, and M. R. Robinson, "Coated nanoparticles and quantum dots for solution-based fabrication of photovoltaic cells," US Patent, US7, 306, 823 B2, 2007.

[3] T. Wada, Y. Matsuo, S. Nomura et al., "Fabrication of Cu(In,Ga)Se$_2$ thin films by a combination of mechanochemical and screen-printing/sintering processes," *Physica Status Solidi (A)*, vol. 203, no. 11, pp. 2593–2597, 2006.

[4] M. Nanu, J. Schoonman, and A. Goossens, "Nanocomposite three-dimensional solar cells obtained by chemical spray deposition," *Nano Letters*, vol. 5, no. 9, pp. 1716–1719, 2005.

[5] T. Ryo, D. C. Nguyen, M. Nakagiri, N. Toyoda, H. Matsuyoshi, and S. Ito, "Characterization of superstrate type CuInS$_2$ solar cells deposited by spray pyrolysis method," *Thin Solid Films*, 2011.

[6] V. K. Kapur, A. Bansal, P. Le, and O. I. Asensio, "Nonvacuum processing of CuIn$_{1-x}$Ga$_x$Se$_2$ solar cells on rigid and flexible substrates using nanoparticle precursor inks," *Thin Solid Films*, vol. 431-432, pp. 53–57, 2003.

[7] Y. Oda, M. Matsubayashi, T. Minemoto, and H. Takakura, "Crystallization of In-Se/CuInSe$_2$ thin-film stack by sequential electrodeposition and annealing," *Journal of Crystal Growth*, vol. 311, no. 3, pp. 738–741, 2009.

[8] D. Lincot, J. F. Guillemoles, S. Taunier et al., "Chalcopyrite thin film solar cells by electrodeposition," *Solar Energy*, vol. 77, no. 6, pp. 725–737, 2004.

[9] T. Halboom, T. Godecke, F. Ernst et al., "Phase relations and microstructure in bulk materials and thin films of the ternary system Cu-In-Se," in *Proceedings of the 11th International Conference on Ternary and Multinary Compounds*, pp. 249–252, Institute of Physics, Salford, UK, 1997.

[10] T. Watanabe, H. Nakazawa, M. Matsui, H. Ohbo, and T. Nakada, "The influence of sodium on the properties of CuInS$_2$ thin films and solar cells," *Solar Energy Materials and Solar Cells*, vol. 49, no. 1–4, pp. 357–363, 1997.

[11] R. Kaigawa, A. Ohyama, T. Wada, and R. Klenk, "Electric properties of Cu-poor and Cu-rich Cu(In,Ga)S$_2$ films after O$_2$-annealing," *Physica Status Solidi (C)*, vol. 3, no. 8, pp. 2568–2571, 2006.

Journal of
Nanotechnology

International Journal of
Corrosion

International Journal of
Polymer Science

Smart Materials Research

Journal of
Composites

BioMed Research International

Journal of
Metallurgy

Journal of
Materials

Hindawi

Submit your manuscripts at
http://www.hindawi.com

Journal of
Nanoparticles

Advances in
Materials Science and Engineering

Scientifica

Journal of
Nanomaterials

The Scientific World Journal

International Journal of
Biomaterials

Journal of
Nanoscience

Journal of
Coatings

Journal of
Crystallography

Journal of
Ceramics

Journal of
Textiles